JOURNAL OF SOLID STATE CHEMISTRY 109, 295–306 (1994)

Quadrupole Interactions and Vibrational Anisotropy of Tetrahedral Fe(III) in the "123" Derivative $LnSr_2Cu_2Ga_{1-x}Fe_xO_7$ (Ln=Y, Ho)

A. Rykov,* V. Caignaert, and B. Raveau

Laboratoire CRISMAT CNRS URA 1318 ISMRA, Universite de Caen, 14050 Caen Cedex, France

Received March 30, 1993; in revised form July 29, 1993; accepted July 29, 1993

The layered copper oxides $LnSr_2Cu_2Ga_{1-x}Fe_xO_7$ (Ln = Y, Ho) have been synthesized for $0 \leq x \leq 1$. An orthorhombic structure (S.G. *Ima*2, $a \approx 22.9$ Å, $b \approx 5.5$ Å, $c \approx 5.4$ Å) forms in the oxides prepared in Ar atmosphere for x rising up to 0.95. The transition from orthorhombic to tetragonal "123" structure (S.G. *P*4/*mmm*, $a_{123} \approx 3.84$ Å, $c_{123} \approx 11.4$ Å) in the range of $0.6 < x < 0.95$ is induced by heating in an oxygen flow. The Mössbauer study reveals that iron exhibits the predominant tetrahedral coordination in the orthorhombic phase, but the pyramidal coordinations in the oxygenated tetragonal $LnSr_2Cu_2FeO_{7.5}$. The characteristic Mössbauer quadrupole doublet associated with the tetrahedral "Ga" site turned out to be asymmetric suggesting an anisotropic thermal vibration of iron in this site. The anisotropy of recoil-free fraction is consistent with a large distortion of the tetrahedral site, where the EFG is parallel to the a direction of the unit cell. The negative sign of V_{zz} and the large value of quadrupole splitting ($|\Delta E_Q| \approx 1.93$ mm/sec) suggest a similarity between the geometry of FeO_4 tetrahedra in both oxides $LnSr_2Cu_2Ga_{1-x}Fe_xO_7$ and $LnBa_2Cu_{3-x}Fe_xO_{-y}$.

1. INTRODUCTION

The study of the substitution of transition elements for copper in the "123" superconductor $YBa_2Cu_3O_{7-y}$ is of great interest for the understanding of the mechanisms of superconductivity in layered cuprates. For this reason a large number of investigations have been performed that deal with the replacement of copper by iron (1–11). In this respect, Mössbauer spectroscopy of ^{57}Fe is an effective tool for probing both the distribution of iron over copper sites and the character of chemical bonding of iron in different coordinations. Recent comprehensive studies of $Y_{1-x}Ca_xBa_2Cu_{3-x}Fe_xO_{7-y}$ by Mössbauer spectroscopy combined with the rationalization of lattice symmetry variations have demonstrated that neither the fourfold planar nor the twofold dumbbell coordinations of copper in Cu(1) site can be adopted by iron located at the Cu(1) level (10). Instead, a pseudotetrahedral coordination of iron has previously been described by several authors in the 123 structure (2–7); pyramidal oxygen environments at the level of the Cu(1) site have also been evidenced (1–8). These different environments of iron produce extended defects that were analyzed on the basis of clustering effects for a significant substitution rate (2–4, 7, 8, 10).

While the relationships between various iron coordinations, oxygen stoichiometry, and lattice symmetry are well understood (4, 10), the origin of unusually large quadrupole splitting for tetrahedral iron sites has not yet been explained. Indeed, no quadrupole splitting for a symmetric tetrahedral coordination (T) can be deduced from a crude point charge model. Large ΔE_Q values, in the 123 structure have been interpreted in terms of square planar (V_4) or "half-pyramidal" (V_4') coordinations of iron (5, 6). Such fourfold coordinations of Fe(III) are unexpected and even unrealistic for solid-state chemists.

In order to get insight into the actual coordinations of Fe(III) it appears interesting to study the substitution of iron for gallium in the 123-type derivative $YSr_2Cu_2GaO_7$. The structure of this phase has been established with accuracy by neutron diffraction (12, 13) showing that gallium exhibits a distorted tetrahedral coordination and is slightly displaced from the ideal Cu(1) site of the 123 structure. Thus, Fe(III) may be an adequate probe of these Ga sites; both Ga(III) and Fe(III) have indeed isotropic d-shells and are characterized by the same trivalent character so that no additional oxygen should be introduced by replacing Ga(III) by Fe(III). Moreover, in $LnSr_2Cu_2GaO_7$ an anisotropy of the thermal vibration ellipsoids of the tetrahedral sites of gallium is expected; however, the anisotropic thermal parameters of this phase were not refined from powder neutron diffraction because of the high complexity of the structure. It is possible to observe an anisotropy of vibrational ellipsoids in Mössbauer spectroscopy since the recoil-free fraction is expected to be anisotropic. Nevertheless, care must be taken to distinguish this effect (14, 15) from the possible preferred orientation phenomena in the polycrystalline sample.

The present work reports on the study of substitution

* On leave from the Institute of Solid State Chemistry, Novosibirsk 630090, Russia.

0022-4596/94 $6.00

of iron for gallium in the oxides $LnSr_2Cu_2GaO_7$ (Ln = Y, Ho) and on the observation of the recoil-free fraction anisotropy for the distorted tetrahedral sites of this structure.

2. EXPERIMENTAL

Enriched (>95%) ^{57}Fe in the form of $^{57}Fe_2O_3$ was mixed in appropriate proportions with Ln_2O_3, $SrCO_3$, CuO, Fe_2O_3, and Ga_2O_3 to obtain the stoichiometry of $LnSr_2Cu_2Ga_{1-x}Fe_xO_7$. The samples were calcined initially in air in 850°C for 24 hr, then ground, heated in air at 950°C for 90 hr, with two intermediate grindings, and quenched into liquid nitrogen. Next, in order to test a possible variation of the iron distribution in the structure we exposed the aliquots of the samples to the oxygenating and reducing treatments denoted [O] and [Ar], respectively. The gas atmosphere specified in square brackets by corresponding symbol referring to three following protocols of gas–heat treatment sequences:

[Air]—heating in air at 950°C, followed by quenching in liquid nitrogen.

[O]—annealing in O_2 gas at 980°C, slow cooling (10°C/hr) to 400°C and oxygenation at 400°C for 12 hr.

[Ar]—annealing at 850°C in flowing Ar gas for 12 hr and cooling to room temperature in Ar.

Mössbauer spectra were recorded at room temperature using a constant-acceleration spectrometer in the time mode and a 512-channel analyzer. Velocity scale calibration and isomer shift reference point were obtained by the room-temperature measurement of the spectra of the α-iron-57 foil. The 0.2-mm thick absorbers with an iron-57 content of about 0.5 mg/cm^2 were prepared by mixing of the samples with MgO in the weight ratio 1 : 1. This procedure avoids the alignment of grains during the filling of sample holder. The complete suppression of preferential orientation in the samples has been verified by recording of spectra in the "magic angle" geometry (16).

The powder X-ray diffraction data were collected by step scanning over an angular range 22–102°(2θ) with increment 0.02°(2θ) by means of high resolution diffractometer "Seifert" using Cu$K\alpha_1$ radiation. The full diffraction profile was analyzed with a modified program DBW (17).

3. RESULTS

3.1. Structural Considerations: X-Ray Diffraction

Starting from the structure of the 123 superconductor $YBa_2Cu_3O_{7-y}$ (Fig. 1a), one can obtain the structure of $YSr_2Cu_2GaO_7$ (Fig. 1b) by simply replacing the rows of CuO_4 square planar groups (labelled Cu1) by rows of corner-sharing GaO_4 tetrahedra. As a result the symmetry

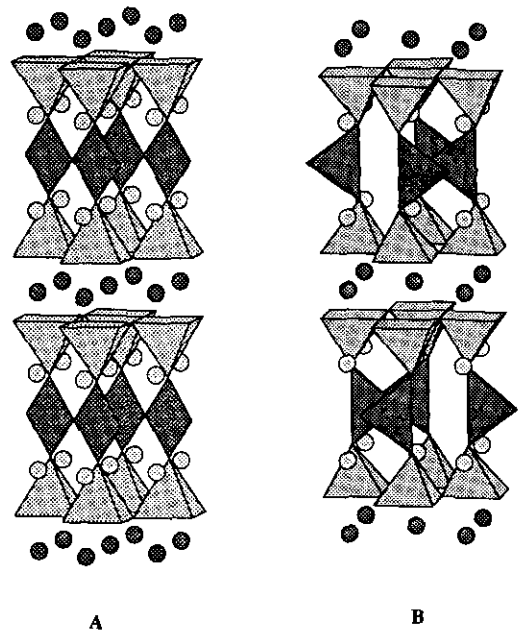

FIG. 1. The crystal structure of (A) $LnBa_2Cu_3O_{6+y}$ and (B) $LnSr_2Cu_2GaO_7$.

of the gallium phase is also orthorhombic (S.G. Ima2), but exhibits parameters different from those of the 123 classical structure with the relations

$$\mathbf{a} = 2\mathbf{c}_{123} \cong 23\ \text{Å}, \quad \mathbf{b} \cong \mathbf{b}_{123}\sqrt{2} \cong 5.5\ \text{Å},$$
$$\mathbf{c} \cong \mathbf{a}_{123}\sqrt{2} \cong 5.4\ \text{Å}.$$

Whatever x, ranging from 0 to 0.95 the oxides $LnSr_2Cu_2Ga_{1-x}Fe_xO_7$ were obtained in the form of single phases with an orthorhombic cell characteristic of the pure gallium cuprate $YSr_2Cu_2GaO_7$ (Table 1). One observes that **a** increases and that the orthorhombic distortion of the perovskite subcell decreases as x increases. This evolution is in accord with the effect of iron which induces a transition from the orthorhombic to the tetragonal symmetry in the 123 structure. Indeed, the oxygen-saturated oxide $YSr_2Cu_2FeO_{7.5}$ (18, 19) and the oxygen-depleted oxide $YSr_2Cu_2FeO_{6.8}$ (19) are both tetragonal with

$$\mathbf{a} = 3.82\ \text{Å} \cong \mathbf{a}_{123};\ \mathbf{c} = 11.34\ \text{Å} \cong \mathbf{c}_{123} \quad \text{for } YSr_2Cu_2FeO_{7.5}$$

$$\mathbf{a} = 3.84\ \text{Å} \cong \mathbf{a}_{123};\ \mathbf{c} = 11.45\ \text{Å} \cong \mathbf{c}_{123} \quad \text{for } YSr_2Cu_2FeO_{6.8}.$$

For comparison the equivalent parameters of the tetragonal cell of the 123-type structure are given in the Table 1 for these new iron-substituted gallium 123 derivatives according to the relations $a_{123} = b_{123} = (b + c)/2\sqrt{2}$;

TABLE 1
Lattice Parameters of the Orthorhombic and Tetragonal Phases of $LnSr_2Cu_2Ga_{1-x}Fe_xO_{7-y}$ (Ln = Y, Ho), Obtained by Thermal Treatments [Air], [O], and [Ar].

Compound	Treatment	a (Å)	b (Å)	c (Å)	a_{123}[a] (Å)	c_{123}[a] (Å)
$YSr_2Cu_2Ga_{0.97}Fe_{0.03}O_7$	[Air]	22.834(1)	5.4761(2)	5.3945(2)	3.8433	11.417
	[O]	22.836(1)	5.4753(2)	5.3930(2)	3.8425	11.418
	[Ar]	22.834(1)	5.4769(2)	5.3943(2)	3.8435	11.417
$YSr_2Cu_2Ga_{0.5}Fe_{0.5}O_7$	[O]	22.878(1)	5.4715(2)	5.3999(2)	3.8436	11.439
	[Ar]	22.876(2)	5.4723(3)	5.4012(3)	3.8444	11.438
$YSr_2Cu_2Ga_{0.2}Fe_{0.8}O_7$	[Ar]	22.910(2)	5.4621(3)	5.4088(3)	3.8434	11.455
$HoSr_2Cu_2Ga_{0.97}Fe_{0.03}O_7$	[Air]	22.811(1)	5.4779(2)	5.3941(2)	3.8438	11.406
	[O]	22.813(1)	5.4775(3)	5.3929(3)	3.8433	11.407
$HoSr_2Cu_2Ga_{0.2}Fe_{0.8}O_7$	[O]	—	—	—	3.8289(3)	11.380(1)
	[Ar]	22.887(1)	5.4605(2)	5.4036(2)	3.8410	11.443
$HoSr_2Cu_2Ga_{0.1}Fe_{0.9}O_7$	[Ar]	22.904(1)	5.4598(2)	5.4070(3)	3.8420	11.452
$HoSr_2Cu_2Ga_{0.05}Fe_{0.95}O_7$	[Ar]	22.906(1)	5.4556(4)	5.4091(4)	3.8413	11.453
$HoSr_2Cu_2Ga_{0.01}Fe_{0.99}O_7$	[Ar]	—	—	—	3.8361(2)	11.448(1)
$HoSr_2Cu_2FeO_7$	[O]	—	—	—	3.8232(2)	11.348(1)
	[Ar]	—	—	—	3.8336(2)	11.426(1)

[a] For the samples with orthorhombic structure a_{123} and c_{123} are calculated as follows: $a_{123} = (b + c)/2\sqrt{2}$; $c_{123} = a/2$.

$c_{123} = a/2$. It is worth pointing out that the equivalent parameters of the corresponding tetragonal subcell of $YSr_2Cu_2Ga_{0.5}Fe_{0.5}O_7$ converge toward those of the tetragonal phase $YSr_2Cu_2FeO_{6.8}$. This is true also for $HoSr_2Cu_2Ga_{1-x}Fe_xO_7$, whose reduced parameters converge with increasing x toward the parameters of $HoSr_2Cu_2FeO_{7-y}$ deoxygenated by [Ar] treatment (Table 1). Moreover, a large range of substitution rates x from 0.6 (±0.1) to 0.97 (±0.02) has been observed with the lattice symmetry depending upon the partial oxygen pressure used for the synthesis. The transition from orthorhombic to tetragonal symmetry occurs at $x = 0.6$ (±0.1) in the [O] samples and at $x = 0.95$ (±0.02) in the [Ar] samples (Fig. 2). Table 1 shows for $x = 0.8$ the parameters of both orthorhombic and tetragonal phases prepared by [Ar] and [O] treatments, respectively. While for the orthorhombic [Ar] phase the reduced parameters $\mathbf{a}_{123}$ and $\mathbf{c}_{123}$ are close to those of the deoxygenated tetragonal 123 phase of the $HoSr_2Cu_2FeO_{7-y}$, the lattice cell constants of the tetragonal [O] phase are significantly lower thereby indicating excess oxygen. However, unlike the tetragonal phases, the variations of the lattice parameters of the orthorhombic phases $LnSr_2Cu_2Ga_{1-x}Fe_xO_7$ are rather small, whatever x. This result suggests a relative constancy of the oxygen content for the orthorhombic structure.

3.2. *Mössbauer Spectra*

3.2.1. Low substitution rates ($x = 0.03$). For the small doping rates, the structure is unchanged and iron is a faithful probe of the original Ga site. The Mössbauer spectra at room temperature (Fig. 3) are very similar for different thermal treatments; this suggests nearly equal distributions and the same chemical state of iron in the "reduced" and "oxygenated" samples. This is consistent with the fact that the oxygen stoichiometry is fixed at 7.0 in $LnSr_2Cu_2GaO_7$. Such a behavior is in contrast to that of Fe-doped $YBa_2Cu_3O_{7-y}$ ($y > 0$), wherein the oxygen content variations strongly influence the Mössbauer spectra (1, 4–8). In spite of this difference, an invariant feature appears for the oxides $LnSr_2Cu_2Ga_{1-x}Fe_xO_7$ and $LnBa_2Cu_{3-x}Fe_xO_{7\pm y}$ that is related to the quadrupole doublet (D) with the largest quadrupole splitting ΔE_Q. Both systems exhibit the same $|\Delta E_Q|$ value of 1.93 ± 0.01 mm/sec for this D iron site; the latter is predominant in the gallium phase and in the deoxygenated 123 cuprate $LnBa_2Cu_{3-x}Fe_xO_{7\pm y}$. In the widely studied 123 phase, the D species were identified previously with tetrahedral iron(III) located at the level of Cu(1) site (10); this assignment is in agreement with the replacement of gallium by iron in $LnSr_2Cu_2Ga_{1-x}Fe_xO_7$.

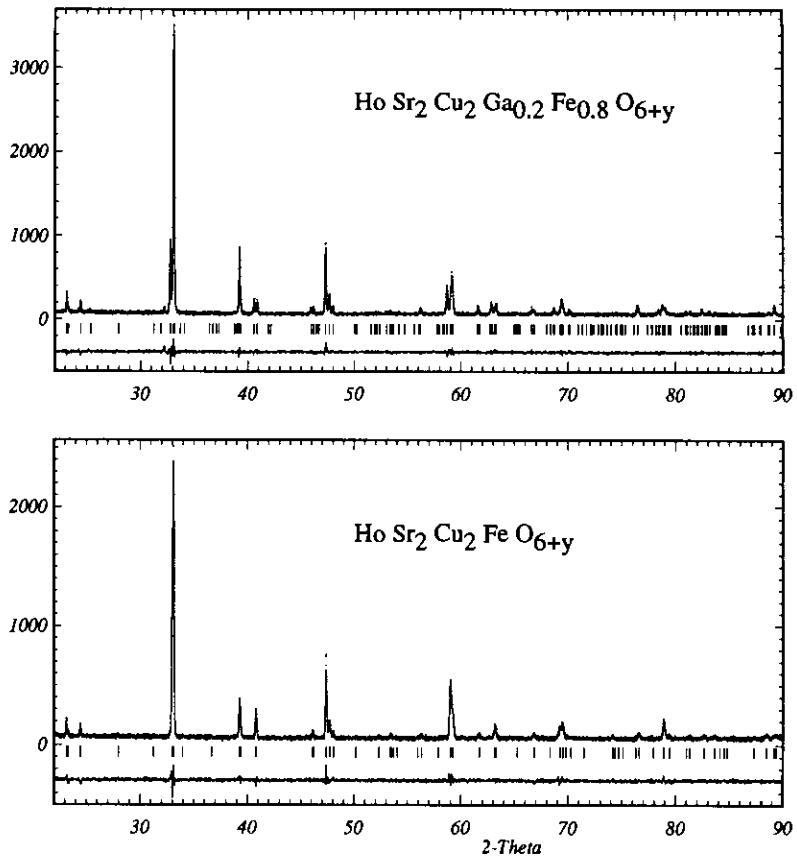

FIG. 2. X-ray diffraction patterns for orthorombic phase $HoSr_2Cu_2Ga_{0.8}Fe_{0.2}O_7$ and tetragonal phase $HoSr_2Cu_2FeO_7$ prepared by [Ar] treatment (see text for details of preparation). Dots represent observed profile; solid lines represent calculated profile and difference.

The spectra of slightly doped samples were evaluated by least squares fitting of Lorenzians with two quadrupole doublets denoted as D ($|\Delta E_Q| \approx 1.93$ mm/sec) and D' ($|\Delta E_Q| = 0.9$–1.2 mm/sec). The percentage of principal D subspectrum reaches 97% in $HoSr_2Cu_2Ga_{0.97}Fe_{0.03}O_7$, allowing its shape to be properly extracted. Because of an obvious spectra asymmetry, the constraints on the equality of linewidth and line intensities were omitted for the principal doublet D. The minor D' component of the spectra was assumed to be symmetric in the final refinement, owing to its small intensity. Thus, ten independent parameters of fit are involved: the total spectral area, the ratio (percentage) of the doublet's area, isomer shifts and quadrupole splittings for each of the two doublets, three full width at half maximum parameters (one for the minor doublet and two for the major one), and the ratio of line intensities $r = I_{3/2}/I_{1/2}$ for the major doublet. These parameters are listed in the Table 2 for the samples prepared by different thermal treatments.

The Mössbauer parameters of the minor D' subspectrum indicate that it originates from iron sitting in the pyramidal; "Cu(2)" copper site. In particular, its chemical shift of about 0.3 mm/sec corresponds to that of iron in Cu(2) site in the 123 structure (10). However, the large linewidth of this subspectrum observed for several samples suggests that there may also exist a contribution of Fe in pyramidal coordination, but located at the level of the Ga sites. The appearance of a second pyramidal coordination for Fe(III) is consistent with its lower affinity for tetrahedral coordination compared to Ga (20).

The analysis of the shape of the principal D doublet has shown that its asymmetry is caused by two effects. First, the integral intensities of the lines corresponding to the transitions $\pm\frac{1}{2} \rightarrow \pm\frac{3}{2}$ and $\pm\frac{1}{2} \rightarrow \pm\frac{3}{2} \rightarrow$ differ by a few percent. Second, we observe that the width of the higher velocity line is systematically larger (Table 2). These two effects were found to be uncorrelated in the different samples. Consequently, they were considered as related to different physical effects. The difference between integral intensities corresponding to the $\pm\frac{1}{2} \rightarrow \pm\frac{3}{2}$ and $\pm\frac{1}{2} \rightarrow \pm\frac{1}{2}$ transitions is attributed to the effect of anisotropy of the Lamb–Mössbauer factor for Fe^{3+}

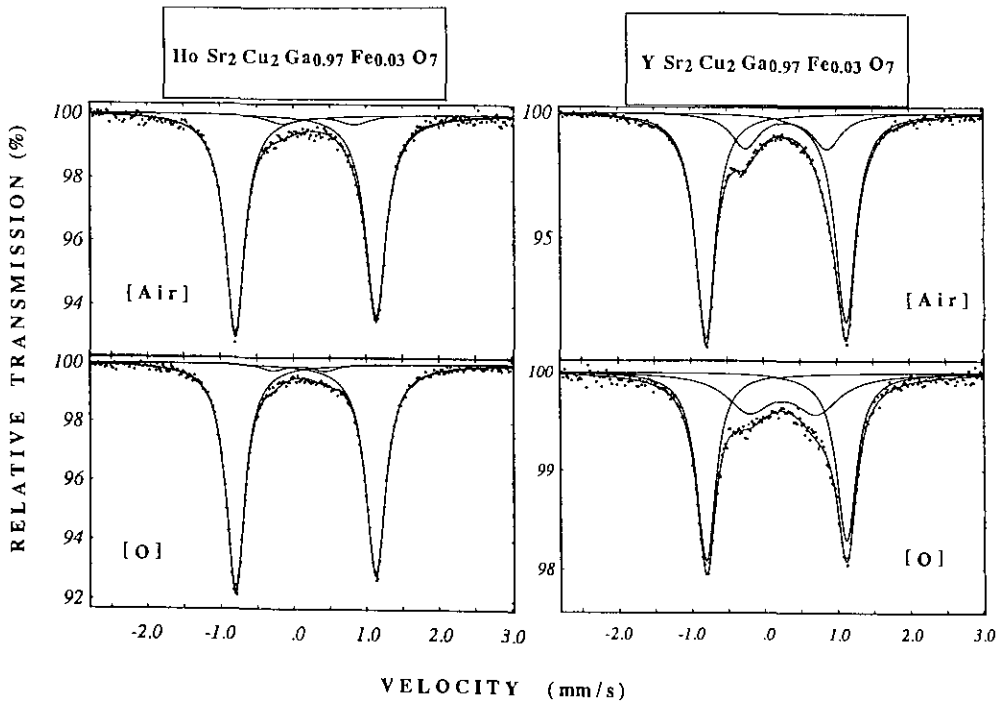

FIG. 3. Room temperature Mossbauer spectra of the samples of the orthorhombic phases $HoSr_2Cu_2Ga_{0.97}Fe_{0.03}O_7$ and $YSr_2Cu_2Ga_{0.97}Fe_{0.03}O_7$, obtained by heat treatments in different gas atmospheres ([O] and [Ar]).

according to Goldanskii et al. (15) and Karyagin (14). On the other hand, the difference between the widths $\Gamma_{3/2}$ and $\Gamma_{1/2}$ cannot be explained by the anisotropy of the thermal vibration ellipsoids. The origin of the asymmetric smearing of the peaks of the quadrupole doublet will be examined further with the study of the deoxygenated phase $LnSr_2Cu_2Ga_{1-x}Fe_xO_7$, heavily doped by magnetic Fe^{3+} ions ($x \geq 0.5$).

The refinement of Mössbauer spectra for low doping rates ($x = 0.03$) allows the degree of vibrational anisotropy for tetrahedral Ga sites to be quantitatively evaluated. For an axially symmetric site in a randomized powder sample the ratio $r = I_{3/2}I_{1/2}$ can be calculated by integration of the intensities of the two lines over all the angles θ between the γ-ray and the principal axis of the electric field gradient (EFG) (21):

$$r = I_{3/2}I_{1/2} = \left(\int_0^1 (1 + \xi^2)\exp(-\alpha\xi^2)d\xi\right) \cdot \left(\int_0^1 (5/3 - \xi^2)\exp(-\alpha\xi^2)d\chi\right)^{-1} \quad [1]$$

with $\xi = \cos\theta$ and where the convenient measure of anisotropy $\alpha = (2\pi/\lambda)^2(\langle \mathbf{u}^2\rangle\| - \langle \mathbf{u}^2\rangle\perp)$, $\langle \mathbf{u}^2\rangle\|$ and $\langle \mathbf{u}^2\rangle\perp$ represent the mean-square vibrational amplitudes parallel and perpendicular, respectively, to the principal EFG axis V_{zz}. When the recoil-free fraction $f = \exp(-(2\pi/\lambda)^2\langle \mathbf{u}^2\rangle)$ is isotropic, then $\alpha = 0$ and relationship [1] gives $I_{3/2}/I_{1/2} = 1$; if $\alpha < 0$ then $I_{3/2}/I_{1/2} > 1$. In our case, the more intense line is lies lower on the velocity scale. This suggests that the sign of V_{zz} is negative ($\Delta E_Q < 0$), and this line corresponds to the $\pm\frac{1}{2} \rightarrow \pm\frac{3}{2}$ transition. Another sign combination compatible with the observation of the more intense left-hand line is $V_{zz} > 0$ and $\alpha > 0$. However, the latter solution can be disregarded since the assumption of a negative V_{zz} is justified by the consideration of both, EFG's sign and vibrational anisotropy in the tetrahedral site of the closely related brownmillerite structure. For instance, in $Ca_2Fe_2O_5$, the local symmetry of the tetrahedral iron site requires that V_{zz} be exactly parallel to the longest **b** axis of the brownmillerite cell. A small value of asymmetry of the EFG tensor and a negative sign of its principal component have been shown by Grant (22). The neutron diffraction study (23) revealed that the thermal vibration tensor is nearly diagonal in the crystalline cell axis with $\langle \mathbf{u}^2\rangle\| < \langle \mathbf{u}^2\rangle\perp$. Moreover, Colville (23) observed a marked distortion of the FeO_4 tetrahedron along the **b** axis, which agrees with a large negative value of V_{zz} along the longest **b** axis. These results lead to the obvious choice $V_{zz} < 0$ and $\alpha < 0$ for the tetrahedral iron

TABLE 2

Isomer Shifts Relative to α–Fe (δ_{IS}), Absolute Value of Quadrupole Splitting ($|\Delta E_Q|$), Full Width at Half-Maximum Linewidths ($\Gamma_{3/2}$ and $\Gamma_{1/2}$), and Relative Spectral Areas (%) of ^{57}Fe Mössbauer Subspectra Observed at Room Temperature in $LnSr_2Cu_2Ga_{1-x}Fe_xO_7$ (Ln = Y, Ho) for Different x Values

Ln	x	Treatment	Subspectra	δ_{IS} (mm/sec)	$\lvert\Delta E_Q\rvert$ (mm/sec)	$\Gamma_{3/2}$ (mm/sec)	$\Gamma_{1/2}$ (mm/sec)	$(I_{3/2}/I_{1/2})^a$	%
Ho	0.03	[Air]	D	0.165(1)	1.934(2)	0.316(4)	0.335(4)	1.033(23)	94
			D′	0.35(3)	0.99(7)	0.51(9)	$=\Gamma_{3/2}$		6
		[O]	D	0.164(1)	1.928(2)	0.307(2)0	0.330(3)	1.010(12)	97
			D′	0.08(2)	0.72(4)	.4(1)	$=\Gamma_{3/2}$		3
Y	0.03	[Air]	D	0.163(1)	1.924(2)	0.316(5)	0.322(3)	1.035(14)	82
			D′	0.316(5)	1.11(1)	0.47(2)	$=\Gamma_{3/2}$		18
		[O]	D	0.163(2)	1.929(4)	0.315(6)	0.328(7)	1.01(5)	65
			D′	0.26(2)	0.93(2)	0.53(3)	$=\Gamma_{3/2}$		35
		[Ar]	D	0.163(2)	1.934(3)	0.342(5)	0.364(5)	1.025(28)	79
			D′	0.319(9)	1.13(2)	0.53(2)	$=\Gamma_{3/2}$		21
Y	0.5	[O]	D	0.168(2)	1.921(3)	0.335(2)	0.326(5)	1.0[b]	74
			D′	0.36(2)	0.99(4)	0.82(5)	$=\Gamma_{3/2}$		26
		[Ar]	D	0.166(3)	1.924(5)	0.466(5)	0.625(7)	1.015(32)	90
			D′	0.27(3)	0.84(7)	0.74(9)	$=\Gamma_{3/2}$		10
Ho	0.6	[O]	D	0.165(2)	1.907(5)	0.38(1)	0.50(1)	1.0[b]	56
			D′	0.046(7)	0.85(3)	0.87(4)	$=\Gamma_{3/2}$		44
		[Ar]	D	0.13(2)	1.82(4)	0.67(3)	1.29(5)	1.0[b]	96
			D′	0.2(1)	0.8(2)	0.9(5)	$=\Gamma_{3/2}$		4
Ho	0.8	[O]	A	0.275(7)	0.53(1)	0.48(2)	$=\Gamma_{3/2}$	1.0[b]	36
			B	−0.031(7)	0.722(8)	0.51(2)	$=\Gamma_{3/2}$	1.0[b]	40
			D	0.158(3)	1.874(8)	0.38(1)	$=\Gamma_{3/2}$	1.0[b]	24
		[Ar]	D[c]	0.159(2)	1.85(1)				100
Ho	1.0	[O]	A	0.285(8)	0.60(1)	0.51(2)	$=\Gamma_{3/2}$	1.0[b]	38
			B	−0.041(7)	0.760(5)	0.55(2)	$=\Gamma_{3/2}$	1.0[b]	62
		[Air]	A	0.283(5)	0.599(9)	0.44(1)	$=\Gamma_{3/2}$	1.0[b]	36
			B	−0.017(7)	0.721(7)	0.52(2)	$=\Gamma_{3/2}$	1.0[b]	47
			D	0.185(8)	1.63(2)	0.49(2)	$=\Gamma_{3/2}$	1.0[b]	17
		[Ar]	A[d]	0.29(1)	0.52(1)				34
			D[c]	0.16(1)	1.9(1)				66

[a] (Lower velocity line area)/(higher velocity line area).
[b] Fixed value.
[c] Magnetically split subspectrum with H_{eff} = 4.0(5) T.
[d] Magnetically split subspectrum with H_{eff} = 35(1) T.

site studied in this work. The values of $I_{3/2}/I_{1/2}$ (Table 2) can be used for the evaluation of the anisotropy of iron vibration ellipsoids at 300 K in the Ga site of $LnSr_2Cu_2GaO_7$. A linear approximation of the integral relationship [1] gives the values of $\alpha \approx 7.5\ ((I_{3/2}/I_{1/2}) - 1)$ in the range of 0.1–0.3, to be compared with the value of $\alpha = 0.1$ for $Ca_2Fe_2O_5$, calculated from neutron diffraction data (23). Our analysis confirms that, like in $Ca_2Fe_2O_5$, the thermal vibrations are much more pronounced in the plane of two shortest cell axes. In the orthorhombic $LnSr_2Cu_2GaO_7$ structure, the orientation of the axis of maximum vibration is away from the strongest Ga bonds which are directed toward the apex of the CuO_5 pyramids.

The second reason for the asymmetry of the D subspectrum is due to the difference of linewidth. Table 2 shows that for all the samples the full width at half maximum $\Gamma_{1/2}$ of the line corresponding to the $\pm\frac{1}{2} \rightarrow \pm\frac{1}{2}$ transition is significantly broader than the width $\Gamma_{3/2}$ of the line corresponding to the $\pm\frac{1}{2} \rightarrow \pm\frac{3}{2}$ transition. In our calibration measurements carried out with an α-Fe foil, the full

width at half maximum of 0.234(1) mm/sec was obtained for the inner two peaks of the six-line spectrum. This suggests that both lines of the quadrupole D subspectrum are slightly broadened at room temperature with respect to the instrumental linewidth. The quadrupole spectrum broadening originates frequently from inhomogeneity of iron environments over the sample, which may lead to a broad distribution of quadrupole splittings ΔE_Q or isomer shifts δ_{IS}. If it is the case, the shape of the spectrum strongly implies a positive correlation between the values of $(\delta_{IS})_i$ and $|\Delta E_Q|_i$ in the distribution. However, more likely, the asymmetric line broadening of the D subspectrum can be correlated to the spin relaxation rate, that slows down. An analogous broadening of the corresponding subspectrum ($\Delta E_Q = 1.94$ mm/sec) has been observed in $YBa_2Cu_{3-x}Fe_xO_{7-y}$ as the temperature decreases from 300 to 78 K (24). The transition rates between electronic levels slows down as T decreases and a differential broadening of the quadrupole lines occurs (25). By analogy with $Ca_2Fe_2O_5$ one can suppose that in $LnSr_2Cu_2Ga_{1-x}Fe_xO_7$ the Fe^{3+} electronic spin relaxes to the plane perpendicular to the longest cell axis. In $Ca_2Fe_2O_5$, H_{eff} is perpendicular to V_{zz} and V_{zz} is negative. Kündig's calculations (26) show that when $V_{zz} < 0$ and $V_{zz} \perp H_{eff}$, the right-hand peak of the doublet broadens first increasing the perturbation energy of the magnetic dipole interactions. Thus, since the electronic spin relaxation rate of Fe^{3+} is conventionally too fast to produce the quadrupole subspectrum asymmetry, our observation suggests a rather unusual character of the electronic spin states in $LnSr_2Cu_2Ga_{1-x}Fe_xO_7$.

3.2.2. High substitution rates. For high substitution rates of gallium by iron a dramatic difference appears between the Mössbauer spectra of samples obtained by [O] and [Ar] thermal treatments (Fig. 4). In the oxygen saturated samples, the population of the tetrahedral iron D species decreases as x increases. The intensities of the two other doublets (A and B) increase at the expense of the D subspectrum, so that for the pure iron members $LnSr_2Cu_2FeO_{7.5}$ one only observes the A and B subspectra. The Mössbauer parameters of these subspectra are the same as the corresponding parameters of A and B subspectra of 123 phase. The A and B species were previously attributed (10) to the pyramidal coordinations of iron in Cu2 and Cu1 sites, respectively. The abrupt increase of the population of iron in both coordinations when $x > 0.5$ is in agreement with the orthorhombic-to-tetragonal transition. This result suggests that the substitution of iron for gallium destabilises the orthorhombic structure; this is in agreement with the ability of iron to exhibit the pyramidal coordination on the Ga sites of the oxygen-saturated samples.

On the contrary, in the [Ar] samples, an overwhelming majority of Fe^{3+} cations remains in the tetrahedral Ga site in agreement with a conservation of the orthorhombic symmetry up to $x = 0.95$. A pyramidal B coordination of iron located at the level of Ga site is, indeed, not possible when the oxygen content is "O_7" or less. Two Mössbauer components are observed in this case: A and D subspectra; they both appear in a magnetically split form. The values of the hyperfine field H_{eff} at room temperature of about 30 T for the A subspectrum are close to that for iron sitting in the Cu(2) sites of the deoxygenated oxide $LnBa_2Cu_{3-x}Fe_xO_{7-y}$ observed earlier (1, 4–6, 24). The temperature of the magnetic ordering in the Cu(2) plane of the 123 structure has been found to increase with decreasing the oxygen content. In the same way H_{eff} increases with increasing x in $LnSr_2Cu_2Ga_{1-x}Fe_xO_{7-y}$, this suggests that at high substitution rates of Fe for Ga the oxygen content decreases below O_7 (Fig. 5). Such an oxygen depletion can be explained by the accommodation of a twofold coordination for a fraction of copper, owing to the redistribution of iron and copper between Ga and Cu sites. The population of iron in the "Cu(2)" sites increases with increasing both, the temperature of deoxygenating treatment and the cooling rate. We observed, that the intensity of A subspectrum can be suppressed by more slowly cooling of the samples at low oxygen pressure. In these conditions the lack of oxygen is reduced and an ideal value of oxygen content 7.0 can be reached.

The origin of the asymmetric line broadening of the D subspectrum is clearly visible in the [Ar]-treated samples. This linewidth asymmetry is explained by slow spin relaxation rate. Two original features of the D subspectrum for $x = 0.5$ support this point of view:

(i) both the $\Gamma_{1/2}$ and $\Gamma_{3/2}$ linewidths increase with reducing treatments;

(ii) the difference between $\Gamma_{3/2}$ and $\Gamma_{1/2}$ increases as $\Gamma_{3/2}$ increases.

Moreover, while for the substitution rate $x = 0.5$ the D subspectrum can be still represented by an asymmetric doublet with a large difference of linewidth, the spectrum for $x = 0.8$ shows a magnetic hyperfine structure, which is consistent with the negative value of ΔE_Q ($\cong -2$ mm/sec) and the low value of H_{eff} (about 4 T). Such an effect suggests that the magnetic fluctuations increase and that the rate of electronic spin relaxation decreases as the substitution rate x increases.

4. DISCUSSION

Shortly after the discovery of the 92 K superconductor $YBa_2Cu_3O_7$, the ^{57}Fe Mössbauer spectra have been widely studied for a large range of substitution, and their "fingerprint" features have been interpreted by many re-

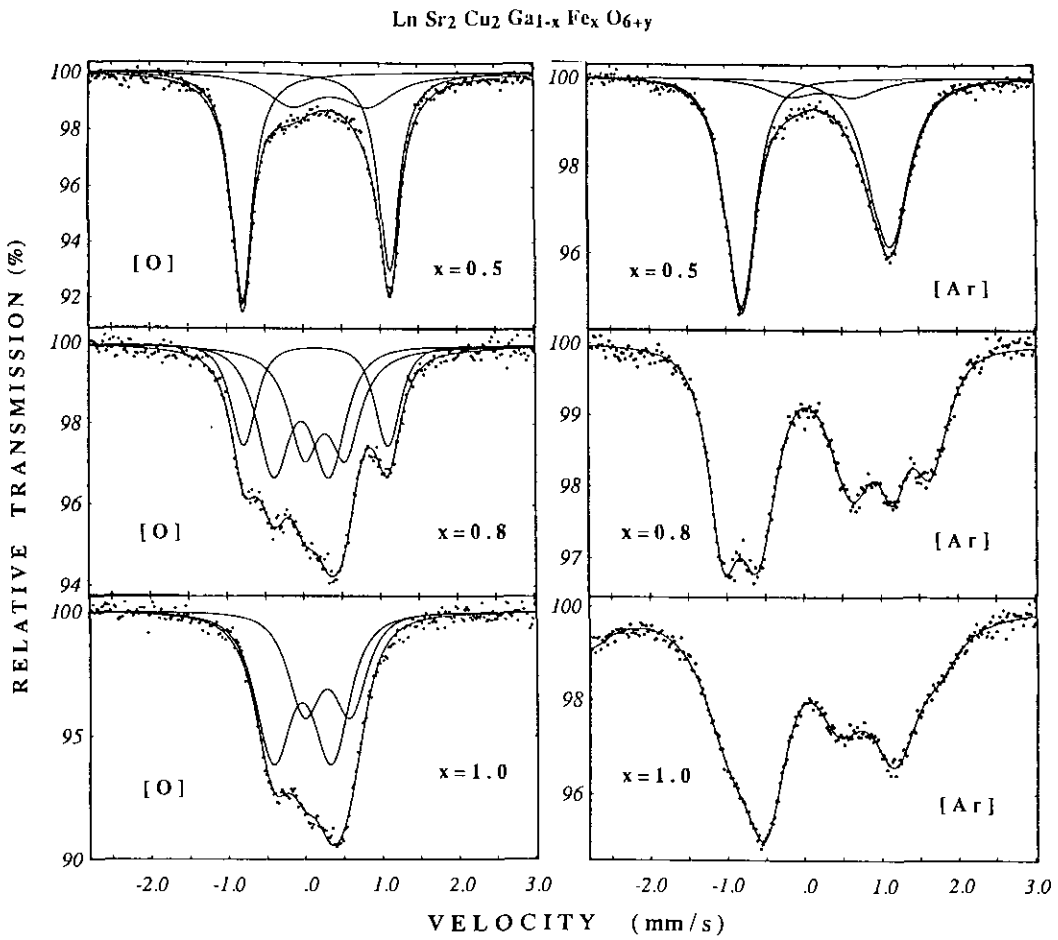

FIG. 4. Room temperature Mössbauer spectra of $YSr_2Cu_2Ga_{0.5}Fe_{0.5}O_7$, $HoSr_2Cu_2Ga_{0.2}Fe_{0.8}O_{6+y}$, and $HoSr_2Cu_2FeO_{6+y}$ obtained by [O] and [Ar] heat treatments.

searchers. However, many of earlier studies have failed even in the identification of Cu1 and Cu2 sites from these spectra because their authors did not realize that the substitutional chemistry of such oxides is extremely complicated. The attribution of the famous four subspectra to proper crystallographic sites, coordination number, valence, and spin state of iron was a rigorous task for Mössbauer experimentalists because of the unusual values of the various subspectra parameters. The reliable data of other methods were necessary to understand this problem. The muon spin relaxation (27) and neutron diffraction (28) observations of antiferromagnetic ordering of copper spins in $YBa_2Cu_3O_6$ allowed an attribution of the minor A subspectrum to the pyramidal Cu2 sites, while the other spectral components (B, C, D) were assigned to different coordinations of iron in the Cu1 site (1, 4–6, 24). Nevertheless, the coordinations, that iron may adopt in the Cu1 sites (Ga sites), as well as oxidation states and electronic configurations of iron remain up to now extremely controversial in the literature.

The assignment of the largest quadrupole doublet (D) to the distorted tetrahedral site (10) provides the next step in the problem. If we turn to the analogous oxides built up on the basis of the perovskite framework, we can find numerous examples of rather high quadrupole splitting for a distorted tetrahedral site. The highly frustrated antiferromagnet $Ca_3Mn_{1.35}Fe_{1.65}O_8$ built up from tetrahedra and octahedra stacked in the sequence OOTOOT shows at room temperature a quadrupole spectrum quite similar to those of Fe-doped $YBa_2Cu_3O_{7-y}$ with $\Delta E_Q = 1.41$ mm/sec for the tetrahedral site (29). The phases $Ca_2LaFe_3O_8$ and $Ca_3Fe_2TiO_8$ with an analogous triple perovskite cell exhibit also rather large values of the quadrupole splittings for both tetrahedral and octahederal iron sites (30, 31). In the simple perovskite $Ca_2Ti_{2-2x}Fe_{2x}O_{6-x}$ ($x \leq 0.5$) the oxygen vacancies form pairs or more extended rods in the vicinity of Fe atoms and again a quadrupole doublet with $\Delta E_Q = 1.5$ mm/sec has been observed for tetrahedral iron (32). This arises the issue of the origin of such a high value of the quadrupole energy and whether it may be

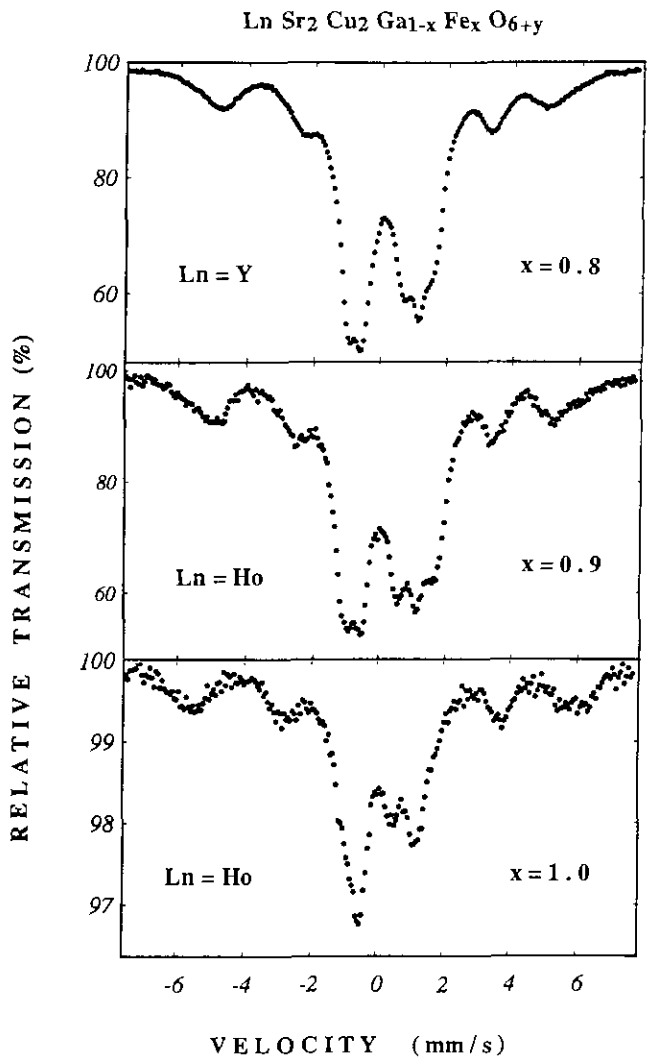

FIG. 5. Room temperature Mössbauer spectra of the samples $YSr_2Cu_2Ga_{0.8}Fe_{0.2}O_7$, $HoSr_2Cu_2Ga_{0.1}Fe_{0.9}O_{6+y}$, and $HoSr_2Cu_2FeO_{6+y}$ prepared by [Ar] treatment.

described in the context of usual point-charge considerations. Bancroft and Platt (33) have reviewed the applications of the point-charge model and found that it works surprisingly well in the limits of a particular family of closely related compounds. This idea stimulates our attempts to consider the ΔE_Q values in relation with the degree of distortion of the Fe tetrahedron.

The values of quadrupole splitting $|\Delta E_Q|$ are quoted in Table 3 for the brownmillerite-related oxides whose structural data are well established by neutron diffraction or single crystal X-ray studies. The degree of distortion of the FeO_4 tetrahedron from its idealized geometry is characterized by the angle θ between two equivalent Fe (III)–O bonds pointing at the apex of the CuO_5 pyramids or the FeO_6 octahedra. The values of $|\Delta E_Q|$ are also given for the ^{57}Fe-doped oxides $LaSrCuGaO_5$ and $LaSrCuAlO_5$ involving CuO_6 octahedra, and the corresponding Mössbauer spectra are shown on Fig. 4. The complete investigation of these systems will be reported elsewhere.

The well-characterized oxides with brownmillerite-related structures provide an illustration of the rather regular relation between $|\Delta E_Q|$ and Θ. The consideration of interatomic distances in these structures shows that the point symmetry of tetrahedron is close to C_{2v}, owing to two short and two long Fe–O bonds. Using the point-charge approach to the case of C_{2v} symmetry it can be shown that for $\Theta > 109.47°$

$$V_{zz} = (3\sin^2(\Theta/2) - 1)[O_\parallel] - [O_\perp] \qquad [2]$$

where $[O_\parallel]$ and $[O_\perp]$ are partial $\langle r^{-3}\rangle$ contributions to V_{zz} from the oxygen pairs parallel and perpendicular to the longest cell axis, respectively. For the Fe–O distances denoted as $r_\parallel$ and $r_\perp$, $|\Delta E_Q|$ increases with Θ as:

$$|\Delta E_Q| \propto 3\sin^2(\Theta/2) - 1 - \langle r_\parallel^3\rangle/\langle r_\perp\rangle^3 \qquad [3]$$

Table 3 shows a straightforward correlation between $|\Delta E_Q|$ and Θ values as it follows from the point-charge model taking into account only the monopolar contribution of nearest neighbors to the electric field gradient. However, the ratio of $\langle r_\parallel^3\rangle/\langle r_\perp\rangle^3$ for Fe–$O_\parallel$ and Fe–$O_\perp$ distances (Table 3) varies in the range 0.9 to 1, whereas the value 0.6 of the third term $\langle r_\parallel^3\rangle/\langle r_\perp\rangle^3$ in the Eq. [3] can be roughly evaluated using a plot of experimental values of $|\Delta E_Q|$ vs angle Θ between $O_\parallel$–Fe–$O_\parallel$ bonds (Table 3). This result suggests that the contributions of the oxygens $[O_\parallel]$ and $[O_\perp]$ to the EFGs on Fe nucleus differ more strongly than predicted by ionic model. Bond length considerations show that the apical oxygens $O_\parallel$ of the CuO_5 pyramids or FeO_6 octahedra are bonded more tightly with the tetrahedral iron than the oxygens $O_\perp$ bridged by two iron atoms in tetrahedral coordination. Therefore, the increase of the covalent character of Fe–$O_\parallel$ bonds may lead to a rapid increase of the $[O_\parallel]$ contribution to EFGs, that demonstrates the limitations of an ionic point charge model.

Thus, the above discussion shows that the lattice contribution to EFGs may be large enough to account for the observed large quadrupole splittings. It has been proposed previously on the basis of EFG calculations (11), that the geometry of the FeO_4 tetrahedron in Fe-doped $YBa^2Cu_3O_7$ is nearly the same as that considered here for $LnSr_2Cu_2Ga_{1-x}Fe_xO_7$. The values of $|\Delta E_Q|$ observed in this work for $LnSr_2Cu_2Ga_{1-x}Fe_xO_7$ coincides with those observed previously in ^{57}Fe–$YBa_2Cu_3O_7$. This confirms

TABLE 3

Mössbauer Quadrupole Splitting $|\Delta E_Q|$ and Structural Parameters for Tetrahedral Site in Closely Related Oxides with Structure Built Up from the OT or OTO slabs of Octahedra (O) and Tetrahedra (T) or from the PTP Slabs of Tetrahedra and Pyramids (P)

Oxide	$\lvert\Delta E_Q\rvert$ (mm/sec)	Ref.	$\langle r_\parallel \rangle$ (Å)	$\langle r_\perp \rangle$ (Å)	Angle θ (degrees)	Ref.
$HoSr_2Cu_2GaO_7$	1.93	this work	1.80	1.875	132.6	(13)
$YSr_2Cu_2GaO_7$	1.93	this work	1.828	1.900	134.4	(12)
$LaSrCuGaO_5$	1.827	this work	1.823	1.84	128.3	(34)
$Sr_2LaFe_3O_8$	1.67[a]	(35)	1.85	1.91	133.5	(36)
Ca_2FeAlO_5	1.5	(22)	1.767	1.831	121.3	(37)
$Ca_2Fe_2O_5$	1.38[b]	(38)	1.844	1.912	123	(23)
$Sr_2Fe_2O_5$	1.3[c]	(39, 40)	1.857	1.89	134[d]	(41)
$LaSrCuAlO_5$	1.19	this work	1.749	1.729	118.7	(42)

Note. $\langle r_\parallel \rangle$ and $\langle r_\perp \rangle$ are the average distances from tetrahedral iron to the oxygens located on the tetrahedron edges parallel and perpendicular, respectively, to the direction of the slabs alternation; Θ is the bond angle $O_\parallel$–Fe–$O_\parallel$ between two Fe–$O_\parallel$ bonds pointing at the oxygens lying on the tetrahedron edge parallel to the direction of the slab's alternation.

[a] Measurement at 450°C.

[b] Measurement at 525°C.

[c] Assuming the 90° angle between the principal EFG axis and the hyperfine magnetic field at the nucleus.

[d] A value reported for the space group *Icm*2, ignoring the disordered displacements of tetrahedral iron atoms (41). Another value Θ of 131.5° can be calculated from the atomic coordinates for the symmetry group *Ibm*2 used in more recent X-ray single crystal work (43). However, the interatomic distances given by the authors (43) do not correspond to their set of coordinate data. The accurate Θ value may be indeed lower than both values 134° and 131.5°.

our previous assignment of the D subspectrum to the distorted tetrahedral coordination of iron (10, 11).

A detailed comparison of the parameters of Mössbauer spectra of the oxides investigated in this work and those of Fe-doped $YBa_2Cu_3O_7$ shows some difference between them. First, the D doublet isomer shift in $LnSr_2Cu_2Ga_{1-x}Fe_xO_7$ of about 0.163 mm/sec (Table 2) is characteristic of tetrahedral Fe(III) (44). This value is higher than the δ_{IS} values observed earlier for the corresponding doublet in Fe-doped $YBa_2Cu_3O_{7-y}$ (1, 24) or $Y_{1-z}Ca_zBa_2Cu_3O_{7-y}$ (10, 11). In these cuprates, the D subspectrum isomer shift varies in the range 0.0–0.1 mm/sec depending on the oxygen content "O_{7-y}." Nath *et al.* (45) and Homonnay *et al.* (46) have investigated the δ_{IS} variation of the corresponding D species (A in their notation) in ^{57}Co-doped $YBa_2Cu_3O_{7-y}$ as a function of oxygen stoichiometry. They have shown that δ_{IS} increases with deoxygenation so that the transition from metal (superconductor) to insulator is reflected in the plot of δ_{IS} vs oxygen content. The increase of δ_{IS} has been explained by the departure of delocalized electrons from Fe 4*s* orbitals. Using the same idea, the increase of δ_{IS}(D) up to 0.16–0.17 mm/sec in $LnSr_2Cu_2Ga_{1-x}Fe_xO_7$ can be explained by still higher electron localization on the 3*d* orbitals, according to fixed stoichiometry of this compound.

The second original feature of our Mössbauer subspectra parameters deals with the pyramidal Cu(2) site. The iron sitting in "Cu(2)" site of $LnSr_2Cu_2Ga_{1-x}Fe_xO_7$ exhibits the same isomer shift as $YBa_2Cu_{3-x}Fe_xO_{7-y}$, but its quadrupole splitting is larger than in the oxygenated superconducting oxides $YBa_2Cu_{3-x}Fe_xO_{7-y}$ and $Y_{1-z}Ca_zBa_2Cu_{3-x}Fe_xO_{7-y}$ (10). However, the apical distance in the CuO_5 pyramids for $LnSr_2Cu_2GaO_7$ is significantly higher than for $LnBa_2Cu_3O_7$. The effect of the elongation of the CuO_5 pyramids on the ΔE_Q has been explained previously (11, 47). Our values of ΔE_Q for the Cu(2) subspectrum in $LnSr_2Cu_2Ga_{0.97}Fe_{0.03}O_7$ are in agreement with the value $|\Delta E_Q|$ = 1.27 mm/sec observed in $La_2CaCu_2O_6$ for CuO_5 pyramids (47). Thus, the dependence of the quadrupole splitting of A subspectrum on the apical distance (10), is confirmed by the present data. It is also clear that for an octahedral coordination of iron in these oxides one observes a low value of the quadrupole splitting (0.3–0.4 mm/sec), as is shown for the internal quadrupole doublet in $LaSrCuGaO_5$ and $LaSrCuAlO_5$ (Fig. 6). This octahedral coordination for $La_2SrCu_2O_6$ produced by oxygen intercalation between of the pyramidal copper layers has been observed earlier by Meyer *et al.* (47). Such an intercalation of an extra-oxygen at the level of Y or Ho layers was not observed here in the oxides $YSr_2Cu_2GaO_7$ and $HoSr_2Cu_2GaO_7$. However, our prelimi-

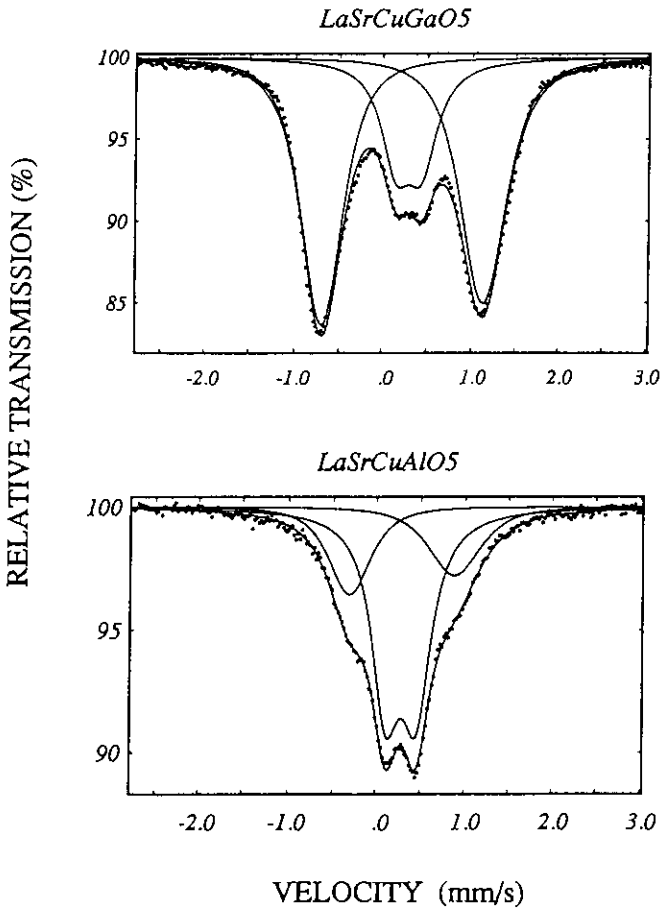

FIG. 6. Mössbauer spectra of the phases $LaSrCuGaO_5$ and $LaSrCuAlO_5$ doped with an Fe rate of 5% of the total number of Cu and Ga(Al) sites.

nary observation of the doublet with $|\Delta E_Q| = 0.4$ mm/sec for Fe-doped $LaSr_2Cu_2GaO_7$ suggests that additional oxygen may be intercalated between the two pyramidal copper layers, owing to the larger ionic size of La. This result is in agreement with the sharp increase of the interlayer distance in the La phase, observed previously by Roth *et al.* (12). A more detailed study of the systems involving an octahedral Fe coordination is in progress.

5. CONCLUDING REMARKS

This study performed on the oxides involving distorted tetrahedral sites occupied by Ga clearly shows that the geometry of the GaO_4 tetrahedron is not perturbed by Fe substitution. Consequently, the observed Mössbauer parameters indicate that the FeO_4 tetrahedra are very similar in both substituted oxides $LnSr_2Cu_2Ga_{1-x}Fe_xO_7$ and $LnBa_2Cu_{3-x}Fe_xO_7$. Thus, the D doublet characterized by the quadrupole splitting $|\Delta E_Q| = 1.95$ mm/sec can be assigned without any ambiguity to the distorted tetrahedral site.

Another important result deals with the first observation of vibrational anisotropy for such a site by Mössbauer spectroscopy. This effect was not observed previously in brownmillerite-related oxides because of the presence of a second octahedral site, producing a quadrupole spectrum with close Mössbauer parameters. The extraction of a Mössbauer subspectrum originating from the tetrahedral iron site only allows a better understanding of iron chemical bonding in oxygen-deficient perovskites built up from the tetrahedra and octahedra or from tetrahedra and pyramids.

REFERENCES

1. Yu. T. Pavlyuhin, N. G. Hainovsky, Y. Y. Medikov, and A. I. Rykov, *Pramana* **31,** L445 (1988).
2. P. Bordet, J. L. Hondeau, P. Strobel, M. Marezio, and A. Santoro, *Solid State Commun.* **66,** 435 (1988).
3. B. D. Dunlap, J. D. Jorgensen, C. Segre, A. E. Dwight, J. L. Matykiewicz, H. Lee, W. Peng, and C. W. Kimball, *Physica C* **158,** 379 (1989).
4. S. Katsuyama, Y. Ueda, and K. Kosuge, *Physica C* **165,** 404 (1990).
5. D. Hechel, I. Nowik, E. R. Bauminger, and I. Felner, *Phys. Rev.* **42,** 2166 (1990).
6. M. E. Lines and M. Eibschutz, *Physica C* **166,** 235 (1990).
7. W. Peng, C. W. Kimball, and B. D. Dunlap. *Physica C* **169,** 23 (1990).
8. M. G. Smith, R. D. Taylor, and H. Oesterreicher, *J. Appl. Phys.* **69,** 4894 (1991).
9. E. Suard, V. Caignaert, A. Maignan, and B. Raveau, *Physica C* **182,** 219 (1991).
10. A. Rykov, V. Caignaert, N. Nguyen, A. Maignan, E. Suard, and B. Raveau. *Physica C* **205,** 63 (1993).
11. A. Rykov, A. Ducouret, N. Nguyen, V. Caignaert, F. Studer, and B. Raveau. *Hyperfine Interact.*, **77,** 277 (1993).
12. G. Roth, P. Adelmann, G. Heger, R. Knitter, and Th. Wolf, *J. Phys. I* **1,** (1991) 721.
13. J. T. Vaughey, J. T. Thiel, E. F. Hasty, D. A. Groenke, Ch.H. Stern, K. R. Poepelmeier, B. Dabrowski, D. G. Hinks, and A. W. Mitchell, *Chem. Mater.* **3,** 1200 (1991).
14. S. V. Karyagin, *Dokl. Akad. Nauk SSSR* **148,** 1102 (1963).
15. V. I. Goldanskii, E. F. Makarov, and U. V. Kharpov, *Phys. Lett.* **3,** 344 (1963).
16. S. Nagy, E. Szilagyi, Y. Wei, and A. Nath, *Struct. Chem.* **1,** 297 (1989).
17. D. B. Wiles and R. A. Young, *J. Appl. Crystallogr.* **14,** 149 (1981).
18. P. R. Slater and G. Greaves, *Physica C* **180,** 299 (1991).
19. M. Pissas, G. Kallias, Z. Simopoulos, D. Niarchos, and A. Kostikas, *Phys. Rev. B* **46,** 14119 (1992).
20. R. W. Grant, H. Wiedersich, S. Geller, U. Gonser, and G. P. Espinosa, *J. Appl. Phys.* **38,** 1455 (1967).
21. P. A. Flinn, S. L. Ruby, and W. L. Kehl, *Science* **143,** 1434 (1964).
22. R. W. Grant, *J. Chem. Phys.* **51,** 1156 (1969).
23. A. A. Colville, *Acta Crystallogr. B Sect.* **26,** 1469 (1970).
24. Yu. T. Pavlukhin, N. G. Hainovsky, Y. Y. Medikov, and A. I. Rykov, *Int. J. Mod. Phys. B* **3,** 711 (1989).
25. G. Clark, G. M. Bancroft, and A. J. Stone, *J. Chem. Phys.* **47,** 4250 (1967).
26. W. Kündig, *Nucl. Instrum. Methods* **48,** 219 (1967).
27. N. Nishida, H. Miyatake, D. Shimada, S. Okuma, M. Ishikawa, T. Takabatake, Y. Nakazawa, Y. Kuno, R. Keitel, J. H. Brewer, T. M. Riseman, D. L. Williams, Y. Watanabe, T. Yamazaki, K. Nishiyama, K. Nagamine, E. J. Ansaldo, and E. Torikai, *Jpn. J. Appl. Phys.* **26,** L1856 (1987).

28. J. M. Tranquada, D. E. Cox, W. Kunnmann, H. Moudden, G. Shirane, M. Suenada, P. Zolliker, D. Vaknin, S. K. Sinha, M. S. Alvarez, A. J. Jakobson, and D. C. Johnston, *Phys. Rev. Lett.* **60,** 156 (1988).
29. N. Nguyen, Y. Calage, F. Varret, G. Ferey, V. Caignaert, M. Hervieu, and B. Raveau, *J. Solid State Chem.* **53,** 398 (1984).
30. J. C. Grenier, J. Darriet, M. Pouchard, and P. Hagenmuller, *Mater. Res. Bull.* **11,** 1219 (1976).
31. J. C. Grenier, F. Menil, M. Pouchard, and P. Hagenmuller, *Mater. Res. Bull.* **12,** 79 (1977).
32. J. C. Grenier, Thèse, Bordeaux, France (1976).
33. G. M. Bancroft and R. H. Platt, *in* "Advances in Inorganic Chemistry and Radiochemistry" **15,** ed. (H. J. Emeléus and A. G. Sharpe, Eds.), Vol. 15, p. 59. Academic Press, New York, 1992.
34. J. T. Vaughey, J. B. Wiley, and K. R. Poepelmeyer, *Z. Anorg. Allg. Chem.* **598/599,** 327 (1991).
35. P. D. Battle, T. C. Gibb, and S. Nixon, *J. Solid State Chem.* **79,** 75 (1989).
36. P. D. Battle, T. C. Gibb, and P. Lightfoot. *J. Solid State Chem.* **84,** 237 (1990).
37. A. A. Colville and S. Geller, *Acta Crystallogr. Sect. B* **27,** 2311 (1971).
38. S. Geller, R. W. Grant, and U. Gonser, *Prog. Solid State Chem.* **5,** 1 (1971).
39. P. K. Gallagher, J. B. MacChesney, and D. N. E. Buchanan, *J. Chem. Phys.* **41,** 2429 (1964).
40. T. C. Gibb, *J. Chem. Soc. Dalton Trans.* 1455 (1985).
41. C. Greaves, A. J. Jacobson, B. C. Tofield, and B. E. Fender, *Acta Crystallogr. Sect. B* **31,** 631 (1975).
42. J. B. Wiley, M. Sabat, S. J. Hwu, and K. R. Poeppelmeier, *J. Solid State Chem.* **87,** 250 (1990).
43. V. M. Harder and Hk. Müller-Buschbaum, *Z. Anorg. Allg. Chem.* **464,** 169 (1980).
44. F. Menil, *J. Phys. Chem. Solids* **46,** 763 (1985).
45. A. Nath, S. Nagy, M. W. Barsoum, S. D. Tyagi, and Y. Wei, *Solid State Commun.* **68,** 181 (1988).
46. Z. Homonnay, A. Nath, Y. Wei, and T. Jing, *Physica C* **174,** 223 (1991).
47. C. Meyer, F. Hartman-Boutron, Y. Gros, and P. Strobel, *Physica C* **181,** 1 (1991).